Reconstructing the Heart Depolarization Pattern from Body Surface Potentials Using Artificial Neural Network

N. A. Mabrouk[1, a], *A. M. khalifa*[1, b] , *A. A. A. Nasser*[2, c] *and Moustafa H. Aly*[2, d]

[1]Department of Electrical Engineering, Faculty of Engineering University Alexandria Egypt, Lotfy El-Sied Rd. off Gamal Abd El-Naser Rd., Alexandria, Egypt
[2]Department of Electrical Engineering, Faculty of Engineering Arab Academy for Science and Technology & Maritime Transport Alexandria Egypt, Abu-Qir, Qism El-Montaza, Alexandria, Egypt
[a]*nihal.ahmed@pua.edu.eg*, [b]*orwa_khalifa@yahoo.com*, [c]*menem_1954@yahoo.com*, [d]*mosaly@aast.edu*

Abstract - *The inverse problem of electrocardiogram (ECG) is an ill-posed problem. Several methods for this problem have been suggested long ago as the regularization technique, with its different types. Artificial neural network technique (ANN) is one of the most important techniques used to solve this problem as it allows a real time solution with minimal processing time. In this paper we present a three-dimensional model of torso-embedded whole heart electrical activity, with spontaneous initiation of activation in the sinoatrial node, showing the electrical activity conduction system throughout the heart. The ANN is trained by data obtained from the forward model by relating the transmembrane potential (TMP) of 58 points distributed all over the heart's surface with body surface potential (BSP) of 81 (9x9) points on the torso's surface. The network is trained by 100 cases each represent a time interval of one millisecond during the depolarization process of 100 milliseconds. This study successfully proves that ANN is able to retrieve the depolarization pattern of the heart at different time intervals. The depolarization patterns of the heart are compared for both the forward and the inverse results at different times. Same steps are repeated for a heart with myocardial infarction. ANN is able to detect the abnormal depolarization pattern and successfully localize the position and size of infarcted region.*

Keywords: Inverse problem, Forward problem, Ill-posed problem, ECG, ANN, TMP, BSP, Myocardial infarction

1.0 INTRODUCTION

Forward and inverse problems are used to describe the performance of physical systems. The forward problem describes the system where the result is determined from the given cause by using a certain fixed mathematical model, while the inverse problem involves the estimation of the cause from the fixed model and the given result [1,3,13]. The inverse problem can be a well-posed or an ill-posed problem.

The problem (A, X, Y) is a well-posed problem, if the following conditions are satisfied:

a) For all $y \in Y$ the equation $Ax = y$ has a solution $x \in X$.
b) The solution is unique.
c) The inverse mapping $A^{-1}: Y \rightarrow X$ is continuous, i.e. the solution x depends continuously on the data y (small errors in y will cause small errors in x).

A problem is called an ill-posed problem, if it is not a well-posed one [2].

The well-posed problem is a solvable problem but the ill-posed one is not the easy problem to be handled, since small errors in the measured data can be critical and introduce large errors in the detected data from the inverse problem. For that reason, we have to find a way to handle this difficulty. There are some regularization techniques, which can approximate ill-posed problems using well-posed equations. There are many regularization techniques like Tikhonov Regularization and the Truncated Singular Value Decomposition [2]. Other techniques like neural network can be used to solve the ill-posed inverse problem. ANN technique is one of the best solutions rather than other mathematical ones, as it allows a real time solution with minimal processing time. [1], [4-17].

The inverse problem of ECG is how to obtain the TMP of the heart from the BSP [18, 21, 22]. To solve the inverse problem of ECG, the problem must be solved first as a forward problem. The forward problem is based on constructing the geometry model including torso and heart. The geometry model is to be solved using a numerical approach based on a set of differential equations and a typical algorithm as the finite element method (FEM) [23].

ANN method is used to solve the inverse problem of ECG using the TMP waves studied on 58 different points spread all over the heart surface. BSP is calculated for each point in the 9x9 array on the torso surface obtained from the forward problem. ANN is used to reconstruct the depolarization pattern of the heart at different milliseconds with time interval of 100 millisecond which is then compared with that obtained from the forward method at the same millisecond. Forward and Inverse steps are repeated for a case of myocardial infarction to check the ability of reconstructing the depolarization pattern and localizing the infarcted region in the heart.

2.0 Methods and Materials

The cardiac torso model introduced in this study compromises a simplified 3D description of the torso and the whole heart including atria, ventricles, and blood chambers, as shown in Figure (1). Dimensions of all shapes were approximated to the real human body dimensions [19].

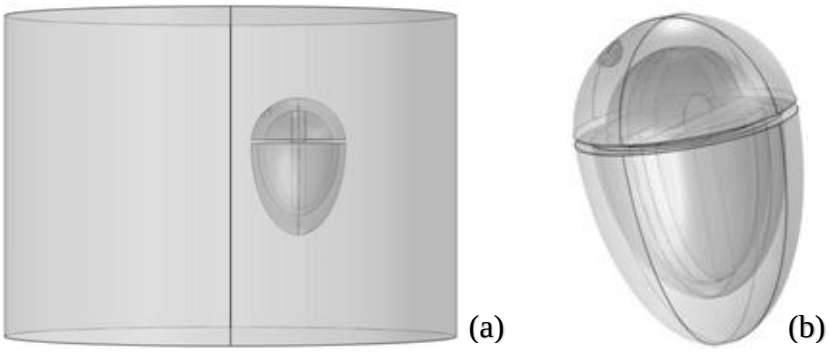

Figure 1: 3D geometry of the torso/heart model (a) and whole heart model (b)

The governing equation for the extracellular voltage V in the passive volume conductor regions (excluding the myocardium) was given by Laplace equation [19,20]:

$$\nabla . (- \sigma_0 \nabla V) = 0, \quad (1)$$

where σ_o is the electrical conductivity of respective outside heart subdomain: torso, and cardiac blood chambers, where $\sigma_{o\ torso} = 0.2$ S/m, $\sigma_{o\ blood} = 0.7$ S/m. All exterior boundaries of the torso were set to be electrically insulating (zero normal component of current density), and all the interior boundaries in contact with the heart were set to $V = V_e$where V_e is the extracellular voltage in the myocardial walls.

The heart is divided into seven subdomains or regions with cardiac cell properties and tissue conductivities representing specialized cells of the conduction system and the myocardium Figure (2). An electrical isolation gap exists between the atria and ventricles except at a junction in the septum that links the atrioventricular node (AVN) with the His bundle [19].

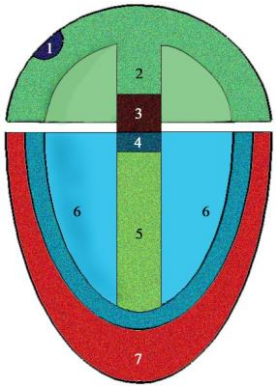

Figure 2: Cross section view of the heart illustrating the various subdomains of the heart. Subdomain numbering is as follows: 1 = sinoatrial node, 2 = atria, 3 = atrioventricular node, 4 = His bundle, 5 = bundle branches, 6 = Purkinje fibers, and 7 = ventricular myocardium.

The model of cellular activation of the heart, including the SAN, is defined at the cellular level by three dependent variables: V_e which is the extracellular potential, V_i Which is the intracellular potential, and u which is a recovery variable governing the cellular refractoriness. The heart equations are based on modified FitzHugh-Nagumo equations [19,20]. For each region of the heart, they are defined according to:

$$\begin{aligned} &\frac{\partial V_e}{\partial t} - \frac{\partial V_i}{\partial t} + \nabla . (- \sigma_e \nabla V_e) = i_{ion} , \\ &\frac{\partial V_i}{\partial t} - \frac{\partial V_e}{\partial t} + \nabla . (- \sigma_i \nabla V_i) = -i_{ion} , \\ &\frac{\partial u}{\partial t} = ke \left[\frac{(V_m - B)}{A} - du - b \right] \end{aligned} \quad (2)$$

where σ_e , σ_i are the extracellular and the intracellular conductivities, respectively, $V_m = V_i - V_e$, where V_m is TMP on the heart surface. and $a, b, c_1, c_2, d, e, k, A,$ and B are region specific parameters.

i_{ion} within the SAN is defined by:

$$i_{ion} = kc_1 (V_m - B)\left[a - \frac{(V_m - B)}{A}\right]\left[1 - \frac{(V_m - B)}{A}\right] + kc_2 u \quad (3)$$

and i_{ion}within the walls of the atria, ventricles, AVN, His bundle, bundle branches, and Purkinje fibers is defined by:

$$i_{ion} = kc_1 (V_m - B)\left[a - \frac{(V_m - B)}{A}\right]\left[1 - \frac{(V_m - B)}{A}\right] + kc_2 u (V_m - B) \quad (4)$$

The values of parameters of the model region-specific are given in Table (1). The parameter e regulates the action potential duration, while the conductivity parameters σ_e , σ_i control the conduction velocities in the tissue. A lower conductivity in the AVN performs an appropriate delay in impulse conduction to the ventricles. The initial values of all model variables are listed in Table (2) [22-25]. Boundary conditions on all interior boundaries in contact with the torso, and cardiac cavities are zero flux for V_i, therefore, −n. Γ=0 where n is the unit outward normal vector on the boundary and Γ is the flux vector through that boundary for the intracellular voltage, which is equal to $\Gamma = -\sigma_i . \frac{\partial V_i}{\partial n}$. For the variable V_e, the inward flux on these boundaries is equal to the outward current density J from the torso/chamber volume conductor; therefore, $-\sigma_e . \frac{\partial V_e}{\partial n} = n . J$. [19, 20].

Table 1: Model Parameters for each region. [19]

Parameter	SAN	Atria	AVN	His	BNL	Purkinje	Ventricles
a	-0.6	0.13	0.13	0.13	0.13	0.13	0.13
b	0.7-0.3	0	0	0	0	0	0
$c_1\ (A.s.V^{-1}.m^{-3})$	1000	2.6	2.6	2.6	2.6	2.6	2.6
$c_2\ (A.s.V^{-1}.m^{-3})$	1	1	1	1	1	1	1
d	0	1	1	1	1	1	1
e	0.066	0.0132	0.0132	0.005	0.0022	0.0047	0.006
$A(mV)$	33	140	140	140	140	140	140
$B(mV)$	-22	-85	+85	-85	-85	-85	-85
$K\ (s^{-1})$	1000	1000	1000	1000	1000	1000	1000
$\sigma_e\ (mS.m^{-1})$	0.5	8	0.5	10	15	35	8
$\sigma_i\ (mS.m^{-1})$	0.5	8	0.5	10	15	35	8

Table 2: Initial variable values for each region. [19]

Parameter	SAN	Atria	AVN	His	BNL	Purkinje	Ventricles
$V_i\ (V)$	-0.06	-0.085	-0.085	-0.085	-0.085	-0.085	-0.085
$V_e\ (V)$	0	0	0	0	0	0	0
u	0	0	0	0	0	0	0

For our case the back propagation artificial neural network was used with 81 input neurons 70 hidden neurons, and 58 output neurons as shown in Figure (3). The input neurons of ANN correspond to the BSP of the 81 points (9x9) array distributed on the torso's surface which is obtained from the forward method and measured at a certain time interval. The output neurons of the ANN correspond to the TMP of the 58 points distributed on the heart surface and also measured at the same time interval. The 81 points of the BSP is shown in figure (4) (a). and the 58 points of the TMP is shown in figure (4) (b). The ANN model is designed to learn the BSP, TMP from 81, 58 points obtained from the results of the forward method. The network was trained by 100 different cases concerning the depolarization of the heart by one millisecond time step. The depolarization pattern retrieved from the ANN is represented on the same geometrical model used in the forward implementation to compare between them at different time points.

For the heart with myocardial infarction to simulate the infarct in the forward method, the intracellular conductivity σ_i , and parameter K where set to zero in the infarcted region, with initial value for V_i and V_e set to -60 mV and -20 mV respectively. The infarct was positioned apically, spanning the epicardium, midmyocardium and endocardium [19].

ANN is examined to detect the size and location of the infarcted region by the same steps used in the normal heart by comparing the depolarization pattern with that obtained from the forward method.

For the forward method, the 3D cardiac model was simulated using COMSOL Multiphysics (COMSOL, v4.4) finite element software. The resulting finite element mesh consists of 141196 tetrahedral elements with 75196 degrees of freedom to be solved at each time step. Each simulation takes approximately 2 hours to solve one second of cardiac activity with 1ms output time resolution. The simulations were performed on an Intel Xeon® E 5640 2.76, 2.66 GHZ PC workstation, with processing power of about 80 Gflops. For the inverse method, we used MATLAB (vR2016a) to create a program using Artificial Neural Network to estimate the TMP from the BSP.

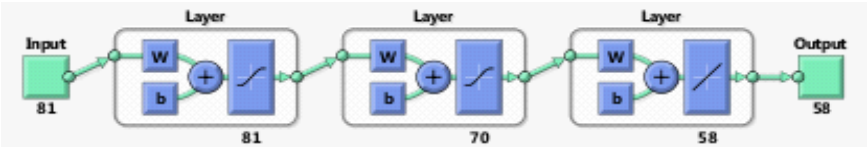

Figure 3: ANN diagram

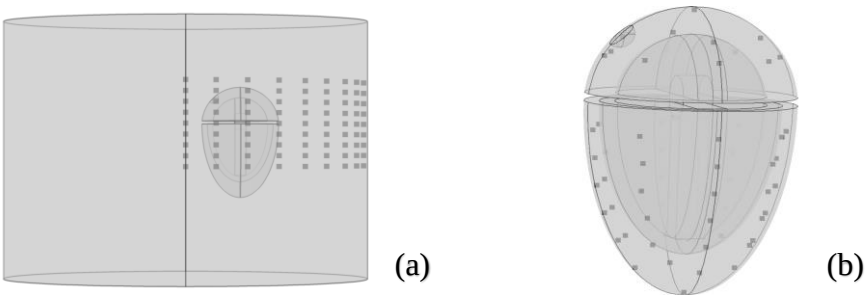

Figure 4: The 81 (9x9) points on the torso's surface(a), and 58 points on the heart's surface(b)

3.0 RESULTS AND DISCUSSION

For the forward simulations, spontaneous and periodic activation begins from the SAN pacemaker region, located in the right atrial wall of the heart. The electrical activation impulse spread from the SAN to the atria and then to the AVN through the atrial septum. The activation spread from the AVN to the His bundle then to the bundle branches, the Purkinje fibers, and at last the whole ventricles at t = 1.321s when the depolarization wave front excites the left and right ventricles as shown in Figure (5).

Figure (6) represents a sample of the BSP, while Figure (7) represents a sample of the TMP at two different points, on the left atrium (a), on the left ventricle (b).

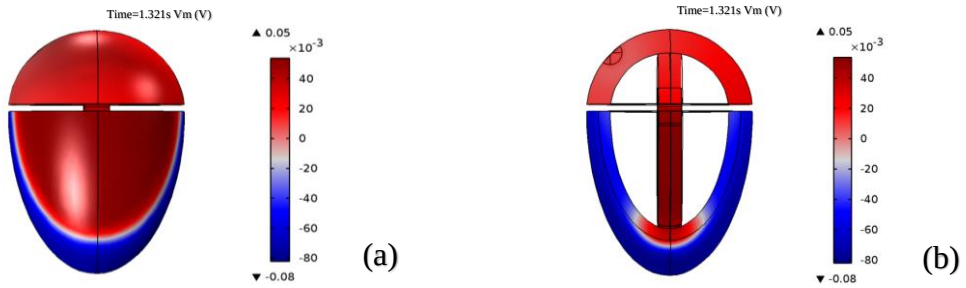

Figure 5: The red color indicates the depolarized region in the heart, (a) V_m on the heart surface, (b) V_m on a frontal plane cross section midway through the heart.

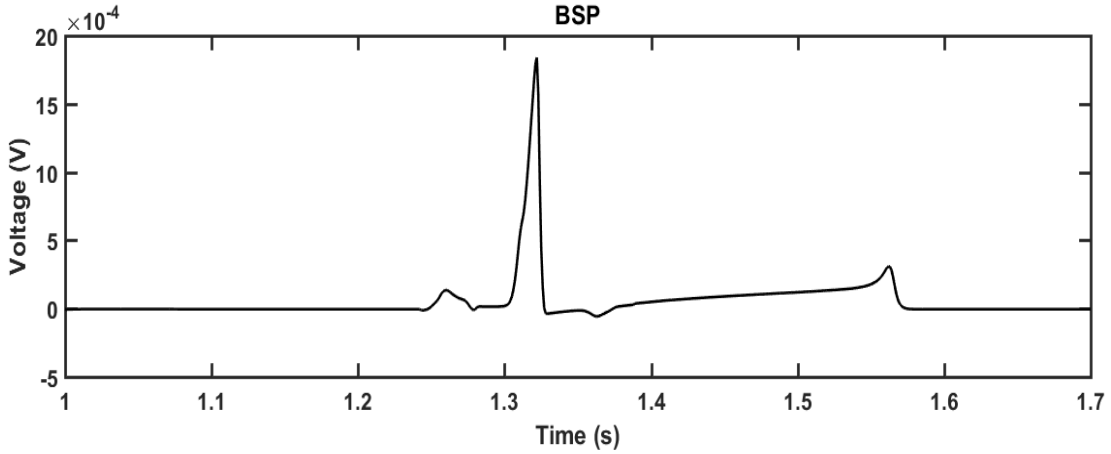

Figure 6: BSP sample on the torso's surface.

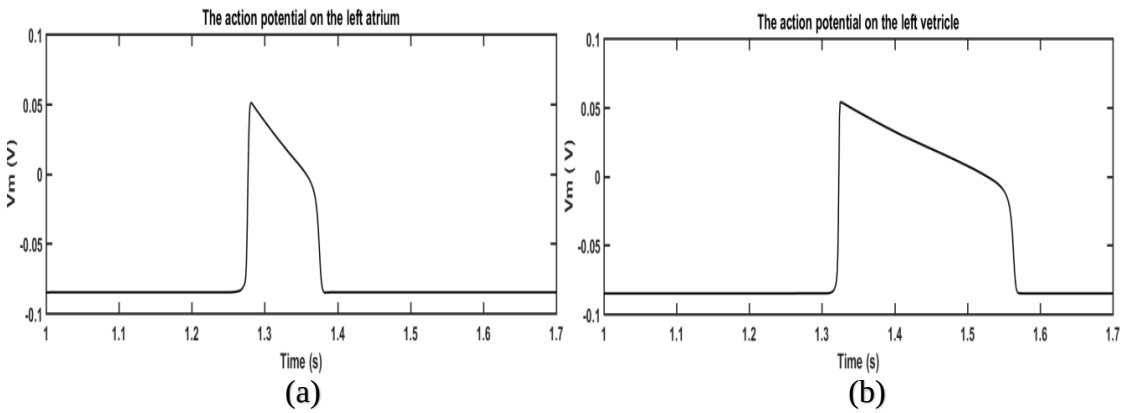

Figure 7: TMP at a point on the left atrium (a), TMP at a point on the left ventricle (b).

Figure (8) shows some samples of the depolarization patterns on the surface of the heart that is simulated in the forward method (a) and reconstructed from the inverse method (b) at three different time points, t = 1.244 s, t =1.28 s, and t = 1.325 s. Figure (9) shows the depolarization patterns in a frontal plane cross section midway through the heart for both the forward method (a), and the inverse method (b) at the same time points. Figure (10) illustrates the depolarization pattern of the heart with MI for both forward and inverse methods. The infarcted region is shown for both forward and inverse method at the epicardial surface (a), and at a cross section midway through the heart (b), when the ventricles are completely depolarized. The simulation indicates the absence of activation in the infarcted region.

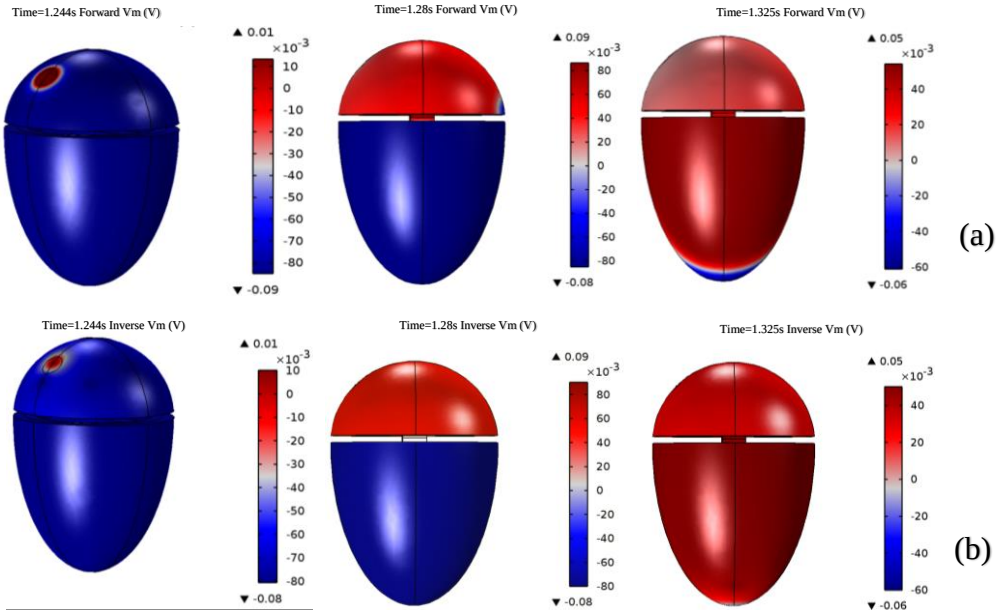

Figure 8: V_m (TMP) on the heart surface at three different time points, (a) for the forward method, (b) for the inverse method.

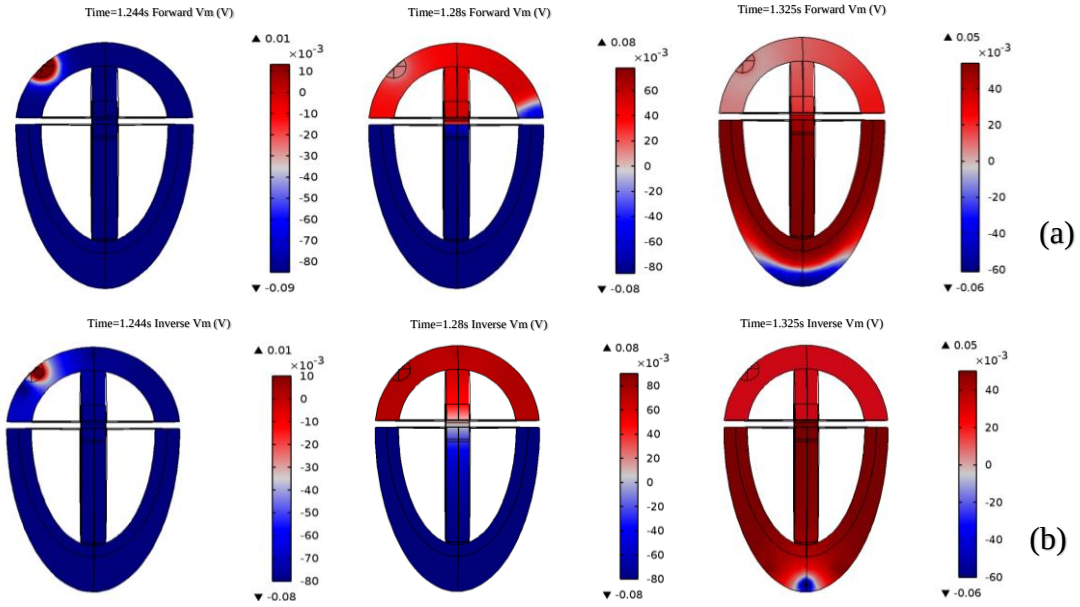

Figure 9: V_m (TMP) in a frontal cross section midway through the heart at three different time points, (a) for the forward method, (b) for the inverse method.

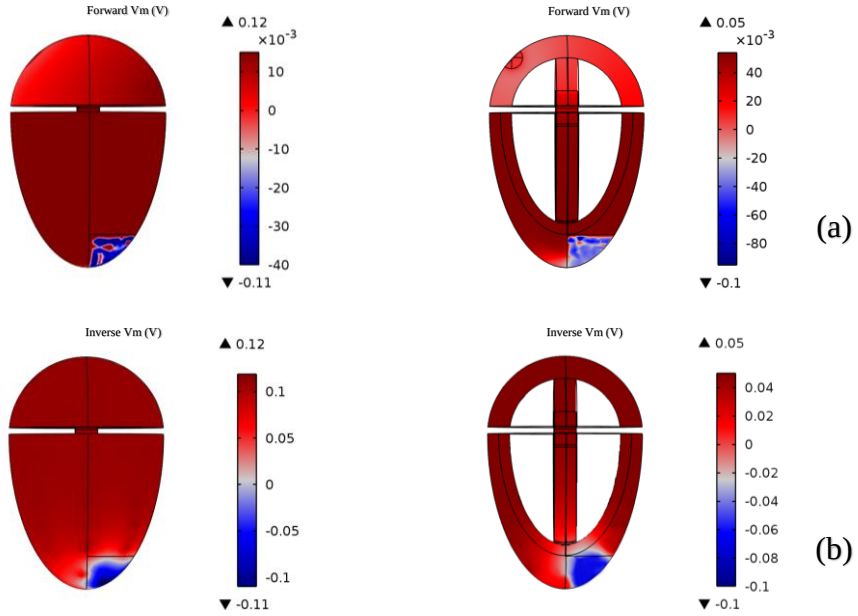

Figure 10: V_m (TMP) of the heart with MI on the heart surface and in a frontal cross section midway through the heart, (a) for the forward method, (b) for the inverse method.

4.0 CONCLUSION

ANN succeeded to reconstruct the depolarization pattern for both normal and myocardial infarcted (MI) heart and locate precisely the infarcted region with an accurate measure for its size. Also, we can conclude that ANN can be used to solve the inverse problem of ECG in real time. The same technique is subjected to further technical trials to detect other cases of MI for different regions and sizes in the heart.

REFERENCES

[1]. I. M. Elshafiey, "Neural network approach for solving inverse problems," MS thesis. Department of Electric Engineering and Computer Engineering, Iowa State University, USA, 1991.

[2]. Mareike. Hullerum, "The inverse problem of electrocardiography: Explanation based on a simple example," Bachelor Thesis, Wilhelms University, Germany, Aug. 2012.

[3]. A. M. Khalifa, "The inverse problem in electrocardiography by using the Fourier transform of the body surface potential: a study on a homogeneous spherical model," In Signal Analysis and Prediction I, EURASIP, ICT Press, Prague, 391-394, June 1997.

[4]. A. M. Khalifa, "The use of neural-network for detection of multi-dipoles in a homogenous spherical conductor: a proposed technique for the inverse problem of electrocardiography," In Signal Analysis and Prediction I, EURASIP, ICT Press, Prague, 395-398, June 1997.

[5]. F. Girosi, M. Jones, and T. Poggio, "Regularization theory and neural networks architectures," Neural Computation 1995, 7, 219-269.

[6]. T. Ogawa, Y. Kosugi, and H. Kanada, "Neural network-based solution to inverse problems," 1998 IEEE International Joint Conference on Neural Networks Proceedings. IEEE World Congress on Computational Intelligence (Cat. No. 98CH36227), 3, 2471-2476, 1998.

[7]. D. Kulkarni, “Solving ill-posed problems with artificial neural networks,” Neural Networks 1991, 4, 477-484.

[8]. A. M. Khalifa, M. A. Razek, and S. Nada, “The ANN as a nonlinear regularization technique to solve the inverse problem of electrocardiography,” Information Technology Applications in Biomedicine. ITAB '97. Proceedings of the IEEE Engineering in Medicine and Biology Society Region 8 International Conference, Prague, Czech Republic, 68-69, 7-9 Sep. 1997.

[9]. C. M. Francesco and C. Maurizio, “Regularization neural networks for inverse problems in non-destructive testing,” in: Nicolet A., Belmans R. Electric and Magnetic Fields, Springer, US, 245-248, 1995.

[10]. G. De Nicolao and G. Ferrari-Trecate, “Regularization networks for inverse problems: A state-space approach,” Automatica 2003, 39, 669-676.

[11]. T. Ogawa and H. Kanada, “Network inversion for complex-valued neural networks,” Proceedings of the Fifth IEEE International Symposium on Signal Processing and Information Technology, Athens, Greece, 850–855, 21-21 Dec. 2005.

[12]. S. Fukami, T. Ogawa, and H. Kanada, “Regularization for complex-valued network inversion,” Proceedings of the SICE Annual Conference, Tokyo, Japan, 1237-1242, 20-22 Aug. 2008.

[13]. T. Ogawa, “Complex-valued neural network and inverse problems,” In Complex-Valued Neural Networks: Utilizing High-Dimensional Parameters, edited by T. Nitta. IGI-Global, 27-55, 2009.

[14]. T. Ogawa, K. Nakamura, and H. Kanada, “Solution of ill-posed inverse problem of distributed generation using complex-valued network inversion,” Proceedings of the international multi-conference of engineers and computer scientists, IMECS 2011, Hong Kong, 16–18 Mar. 2011.

[15]. V. I. Gorbachenko, T. V. Lazovskaya, D. A. Tarkhov, A. N. Vasilyev, and M. V. Zhukov, “Neural network technique in some inverse problems of mathematical physics,” Proceedings of the 13th International Symposium on Neural Networks, ISNN 2016, 310-316, St. Petersburg, Russia, 6-8 July 2016.

[16]. K. H. Jin, M. T. McCann, E. Froustey, and M. Unser, “Deep convolutional neural network for inverse problems in imaging,” IEEE Trans. Image Process. 2017, 26, 4509-4522.

[17]. J. Adler and O. Öktem, “Solving ill-posed inverse problems using iterative deep neural networks,” Inverse Problems 2017, 33, 1-24.

[18]. M. Jiang, S. Jiang, L. Zhu, Y. Wang, W. Huang and H. Zhang, “Study on parameter optimization for support vector regression in solving the inverse ECG problem,” Computational and Mathematical Methods Medicine 2013, 2013, ID 158056, 1-9.

[19]. S. Sovilj, R. Magjarevi´c, N.H. Lovell and S. Dokos, "Simplified 3d model of whole heart electrical activity and 12- lead ECG generation", Computational and Mathematical Methods in Medicine 2013, 2013, ID 134208-10, 1-10.

[20]. S. Dokos, S.L. Cloherty and N.H. Lovell, “Computational model of atrial electrical activation and propagation”, Proceedings of the 29th Annual International Conference of the IEEE EMBS, Lyon, France, 2007, pp. 908-911.

[21]. S. Sovilj, V. Čeperič and P. R. Magjarevič, “3D cardiac electrical activity model”, Automatika 2016, 57, 540-548.

[22]. C. E. Chavez, N. Zemzemi, Y. Coudière, F. Alonso-Atienza, C. E. Chavez, N. Zemzemi and D. Alvarez, “Inverse problem of electrocardiography: estimating the location of cardiac

isquemia in a 3D geometry", functional imaging and modelling of the heart (FIMH2015), Maastricht, Netherlands. Springer International Publishing, 9126, 393-401, 2015.

[23]. G. Shou, L. Xia, M. Jiang, F. Liu, & S. Crozier, "Forward and inverse solutions of electrocardiography problem using an adaptive BEM method," Proceedings of the 4th International Conference on Functional Imaging and Modeling of the Heart, FIMH'07, Salt Lake City, UT, USA, 290–299, 7-9 June, 2007.